Environmental Science Nano

How Nanoscale Surface Heterogeneity Impacts Transport of Nano- to Micro-Particles on Surfaces under Unfavorable Attachment Conditions

Journal:	*Environmental Science: Nano*
Manuscript ID	EN-ART-03-2019-000306.R1
Article Type:	Paper
Date Submitted by the Author:	21-Apr-2019
Complete List of Authors:	Ron, Cesar; University of Utah VanNess, Kurt; University of Utah Rasmuson, Anna; University of Utah Johnson, W.; University of Utah,

Environmental significance statement

Nanoscale heterogeneity on environmental surfaces governs the retention of nano- and micro-particles (colloids) in flowing solution. Understanding this influence is critical to predicting transport in contexts spanning water resource protection to remediation of groundwater via targeted delivery of reactive agents. Combined experiments and mechanistic simulations described herein demonstrate how nanoscale heterogeneity interacts with diffusion, sedimentation and fluid drag to further reduce attachment of 0.2 to 2 μm colloids (n-μ transition) under unfavorable relative to favorable attachment conditions. These findings identify a novel transport attribute that suggests strategies for targeted colloid delivery in environmental contexts. Furthermore, simulations incorporating discrete representation of nanoscale heterogeneity in transport simulations captured the novel transport behavior. This discrete representation serves as a guide to surface characterization studies, elucidating the expected scales and spatial frequencies of nanoscale heterogeneity relevant to colloidal transport.

Draft for Environmental Science: Nano

How Nanoscale Surface Heterogeneity Impacts Transport of Nano- to Micro-Particles on Surfaces under Unfavorable Attachment Conditions

Cesar A. Ron[1], Kurt VanNess[1], Anna Rasmuson[1], William P. Johnson[1]*.

[1]Department of Geology & Geophysics, University of Utah, Salt Lake City, UT 84112, USA

*Corresponding author. Email: william.johnson@utah.edu. Tel.: +1 801 585 5033. Fax: +1 801 581 7065.

Abstract

The impact of nanoscale surface heterogeneity on retention of nano-to-micro-scale particles (colloids) on surfaces governs colloid transport in the environment where unfavorable conditions (repulsive barrier present) are prevalent. Applications include water resource protection and contaminant remediation, and colloid sizes range from viruses and engineered nanomaterials (e.g., ~50 nm) to protozoa and activated carbon (e.g., ~5 μm). Prediction and colloid delivery require understanding how nanoscale heterogeneity impacts size dependence of colloid retention under unfavorable relative to favorable conditions. This dependence has not been previously investigated. We report experiments on soda lime glass (silica) with carboxylate-modified polystyrene latex colloids (0.1, 0.25, 1.1, 2.0, 4.4, 6.8 μm) under varied ionic strengths (0.006 and 0.02 M) and pH (6.7 and 8.0) in an impinging jet system representing upstream sides of porous media grains. These experiments demonstrate dramatically reduced attachment efficiencies (α) for n-μ transition colloids (0.2 to 2 μm) relative to smaller (e.g., < 0.2 μm) or larger (e.g., > 2 μm) sizes with equivalent surface properties. We demonstrate via mechanistic trajectory simulations incorporating discrete representative nanoscale heterogeneity (DRNH) that for n-μ transition colloids, their least combined diffusion and fluid drag in the near-surface fluid domain increased their residence times prior to encountering nanoscale heterogeneity, both phenomena thereby reducing the likelihood of colloid attachment under unfavorable conditions. The generality of this phenomenon was examined using silica colloids, and by compiling reported colloid retention in porous media. We discuss how this new understanding may guide strategies for targeted delivery of in porous media.

Key words: colloid transport, colloid retention, collector efficiency, nanoscale heterogeneity, diffusion, sedimentation, fluid drag.

Introduction

Understanding the retention of nano- and micro-particles (colloids) on environmentally relevant surfaces in flowing solution is critical to contexts spanning water resource protection (e.g., pathogens mobilized during heavy rainfall) to remediation of groundwater via targeted

delivery of reactive agents (e.g., zero valent iron nanoparticles). That colloid retention is greater under favorable (repulsive barrier absent) versus unfavorable (repulsive barrier present) conditions has been long recognized and explored.[1–5] Colloid retention is quantified as collector efficiency (η), which is the ratio of retained relative to introduced colloids in a given collector geometry, with attachment efficiency (α) being the ratio of η under unfavorable (η_{unf}) relative to favorable (η_{fav}) conditions. Mechanistic prediction of colloid attachment under unfavorable conditions (η_{unf} and α) has not been possible without explicit recognition of the role of nanoscale heterogeneity[1], and only recently has data emerged indicating that α is exaggerated for colloids in the size range between approximately 0.2 μm and 2 μm in diameter, as demonstrated for carboxylate-modified polystyrene latex colloids (CML) on silica at pH 8.0 and 6.0 mM NaCl.[6]

The exaggerated minimum η under unfavorable conditions suggests a strategy for enhancement of colloid transport for purposes of targeted delivery to surfaces. The underlying nanoscale interactions, however, must be understood in order to predict and utilize this characteristic. The observed minimum η under favorable conditions is well understood, and is driven by physical transport processes; i.e., advection, settling and diffusion that bring colloids into proximity where they intercept the collector surface.[1,7,8] The colloid size range with lowest η under favorable conditions (e.g., *ca.* 1 μm) has the least combined diffusion and settling, as captured in colloid filtration theory.[7,9–13]

In contrast to favorable conditions, the exaggerated minimum η under unfavorable conditions reflects complex repulsive interactions between colloids and surfaces. Repulsion between surfaces under unfavorable conditions arises predominantly from electric double layer interactions (EDL) for like-charged colloids and collectors.[12–17] Repulsive surfaces (like-charged according to measured bulk surface properties), have nanoscale heterogeneity that drives colloid attachment despite overall repulsion.[1,18,19] Characteristics contributing to surface heterogeneity may include ζ-potential, Hamaker constant, Lewis acid-base characteristic, nanoscale roughness, among others.

Whereas detection of nanoscale heterogeneity is possible using current analytical capabilities (e.g., electrophoresis, x-ray photoelectron spectroscopy, AFM force volume, or other techniques)[16,20–22] the scale of heterogeneity detected will depend on the resolution of tha analysis, and only beyond certain scales and spatial densities of attractive and repulsive domains will heterogeneity actually influence colloid transport. Various surface-sensitive techniques among microscopic, spectrometric, potentiometric, physicochemical adsorption, and others can identify spatial variation in topography[6], chemical composition[23], surface charge[24], and propensity to sorb.[25] The significance of this nanoscale heterogeneity differs with the scale of interacting moieties; i.e., sparse molecular-scale charge heterogeneity may be significant to adsorption of molecules, but may not be significant to attachment of micro-scale colloids. The zone of colloid-surface interaction (ZOI) scales with Debye length and colloid size[26], ranging from ~15 nm (0.1 μm diameter CML, 6 mM, pH 6.72) to ~115 nm (6.8 μm diameter CML, 6mM, pH 6.72), far larger than molecular scales. To allow attachment, colloid-surface interaction must be net attractive[26]; that is, the scale of heterogeneity within the ZOI must be large enough to yield net attraction. The measurement most relevant to colloid transport; i.e., colloidal force measurements at high spatial density across surfaces, also show spatial variation.[21,22] However, even these most relevant measurements lack the requisite resolution to define the scales and spatial densities of nanoscale heterogeneity relevant to colloid transport.

To determine the scales and spatial densities of nanoscale heterogeneity relevant to colloid transport, discrete representation of nanoscale heterogeneity (DRNH) was developed for mineral surfaces.[12,13] The basis for DRNH is that as colloids move into proximity with heterodomains (nanoscale zones of opposite charge to bulk surface), colloid surface interaction will be net repulsive or net attractive depending on the fraction of the ZOI occupied by heterodomain(s).[26] Because ZOI increases with colloid size, and contracts in response to increased ionic strength (IS), colloid-collector interactions depend on colloid size and solution IS, thereby allowing DRNH (heterodomain size distribution and spatial density) to be backed out from arrays of experiments varying these parameters. DRNH was thus determined via leveraged particle trajectory simulations and transport experiments, under varied colloid sizes,

fluid velocities, ionic strengths (IS), and pH values.[12,13] Because of the above-described challenges in direct characterization of nanoscale heterodomain sizes let alone physicochemical characteristics driving nanoscale attraction (ζ-potential, Hamaker constant, etc.), for the sake of parsimony we represent nanoscale heterogeneity using ζ-potential, while admitting that other forms may contribute to nanoscale attraction.

Shave et al.[27] recently showed that 1 μm colloid attachment was faster when DRNH was placed on the collector rather than the colloid surface (due to the impact of colloid rotation). As described above, nanoscale interactions drive lower values of η under unfavorable conditions for n-μ transition colloids, suggesting that the influence of heterogeneity on colloids versus collectors described by Shave et al.[21] may be most dramatic for n-μ transition colloids relative to smaller nanoparticles or larger micro-particles.

Our objective is to demonstrate and mechanistically explain the nanoscale interactions that yield exaggerated minimum η under unfavorable relative to favorable conditions for the *n*-μ transition colloids. Our primary hypothesis is that for n-μ transition colloids, the exaggerated minimum η under unfavorable conditions is driven by the lower combined diffusion, settling and fluid drag operating in two regions: 1) In bulk fluid, least combined diffusion and sedimentation limits colloid delivery to the collector surface as described in CFT, yielding the observed minimum η under favorable conditions; and 2) In near-surface fluid, least combined diffusion and fluid drag limits the likelihood of finding heterodomains on which to attach under unfavorable conditions, exaggerating η_{unf} relative to η_{fav}. Our corollary hypothesis is that the difference in η under unfavorable relative to favorable conditions is decreased for the; e.g., < 0.2 μm and > 2 μm colloid size ranges because of their relatively greater combined diffusion, settling, and fluid drag.

Methods

Colloidal Suspensions

Experiments examined carboxylate-modified polystyrene latex (CML) fluorescent (λ_{ex} = 505, λ_{em} = 515 nm) microspheres (Molecular Probes Inc., Eugene, OR) of six sizes (0.1, 0.25, 1.1, 2.0, 4.4 and 6.8 μm). Microspheres with contrasting properties (e.g., density, hydrophobicity, rheology); i.e., fluorescent (λ_{ex} = 485, λ_{em} = 510 nm) carboxylate-modified silica (CMS) and unmodified silica (UMS) (Creative Diagnostics, Shirley, NY). CMS of two sizes (1.0 and 3.0 μm), and UMS of one size 3.0 μm, were also examined. Colloid suspensions were prepared from stock in relevant solution with concentrations ranging from 2.5×10^5 to 2.5×10^7 microspheres per mL. The microsphere suspension concentration was determined via vacuum filtration of colloid solution (volume adjusted to ensure > 20 CML per observation area) on 0.05 or 0.1 μm polycarbonate filters (Millipore) followed by averaging counts of 45 random observation areas using wide-field fluorescence for colloid illumination and scaling this average to the area of deposition on the filter.

Suspension ionic strength (IS) was adjusted using NaCl. Unfavorable solutions (IS 6 mM and 20 mM) were buffered with 2.2 mM MOPS (3-Morpholinopropane-1-sulfonic acid) (Sigma-Aldrich Corp.) with pH set to 6.7 and 8.0 using NaOH (0.5 M). The ion contribution from the buffer was accounted for when calculating the solution ionic strength. Favorable solutions were achieved by increasing the solution ionic strength to 50 mM and decreasing the pH to 2.0 using HCl (1.3 M). In cases where ζ-potentials of the collector and colloid were both slightly negative, the net interaction was attractive.[6]

CML, CMS and UMS electrophoretic mobility (EPM) was measured in suspensions using ζ-potential analyzer (Mobiuζ, Wyatt Technology Corp., Santa Barbara, CA). CML, CMS and UMS ζ-potentials were calculated from EPM via the Smoluchowski equation[28] (SI, Table SI-1).

CML roughness was measured with an atomic force microscope (model N9451A Agilent Technologies; Santa Clara, CA). CML RMS roughness was 13.0 ± 7.0 nm (1.1 μm), 10.0 ± 7.0 nm (2.0 μm), 13.0 ± 6.0 nm (4.4 μm), and 27.0 ± 9.0 (6.8 μm).[29]

Collector Surface

Soda-lime glass (herein referred to silica) slides and coverslips (Fisher Scientific, Inc.) were used as the impinging surface in the impinging jet flow cell. Silica slides were cleaned via the SC-1 procedure[30] prior to every experiment. Silica ζ-potentials were adopted from representative values reported in the literature[10,31] (SI, Table SI-2).

Silica RMS roughness was 1.0 ± 0.7 nm as measured with an atomic force microscope (model N9451A Agilent Technologies; Santa Clara, CA).[29]

Impinging Jet Experiments

A custom-made stainless-steel impinging jet flow cell (radially symmetric) (SI, Figure SI-1) was used to observe colloid attachment and detachment, as described in previous studies. [6,12,13] The jet (cell inlet) was 0.5 mm in radius, and the impinging surface was located 1.25 mm from the jet, perpendicular to the jet axis. To ensure an evenly radial distribution of the flow across the cell, four outlets were evenly spaced in a circular array at a radial distance 10.0 mm from the jet axis.

Colloid attachment experiments were conducted by injecting colloidal suspensions in the flow cell after 30 min of equilibration of the collector surface with colloid-free solution and attachment was quantified as collector efficiency (η = number attached/number injected).[6,12] Experimental conditions examined the following conditions: pH 6.7 and 8.0, IS 6.0 mM and 20.0 mM, and average jet velocity (v_{jet}) of 1.7E-3 ms^{-1}. The duration of the experiments ranged from 1 to 6 h depending on rate of attachment. Colloids were illuminated using wide-field fluorescence with a band-pass filter for excitation (478-493 nm) and a (405/488/543 nm) dichroic filter for emission (Chroma Technology Corp., Bellows Falls, VT). The 1.1 μm and larger CML were experimentally-observed using a 10x objective (Nikon, Japan), the 3.0 μm CMS and 3.0 μm UMS were observed using a 20X objective (Plan Fluor DIC M/N2; Nikon, Japan), finally the 0.25 μm and smaller CML as well as 1.0 μm CMS were observed using a 60X objective (Plan Apo TIRF DIC H; Nikon, Japan). The number of attached colloids at several time intervals (e.g., 15 s) was tracked with images taken via a CoolSNAP HQ CCD camera (Photometrics, Tucson, AZ) and processed using image analysis software (MetaMorph, Universal Imaging Corp.,

Downingtown, PA). A detailed description of the optical setup is provided in previous publications.[6,10,12,13]

Colloid Trajectory Model

A Lagrangian colloid trajectory model developed for the impinging jet system (e.g., Pazmino et al.[12]) was used to simulate CML trajectories. The model predicts delivery to the surface and attachment if the arresting torque exceeds the driving torque when the colloid is in contact with the surface.

Simulated colloid trajectories are generated in response to Lagrangian integration of forces and torques acting on colloids; i.e., fluid drag, colloid-collector surface interactions (XDLVO), lift, Brownian diffusion, virtual mass, and gravity, as described in previous publications.[6,12,32,33] Colloid-collector surface interaction forces include van der Waals (vdW), electric double layer (EDL), and Born interactions as described in previous publications[6,12,32], whereas Lewis acid-base, steric forces, and roughness impacts, were more recently incorporated.[29,33]

Nanoscale surface roughness has been shown to affect colloid-surface interactions[34,35]. For this reason, a modification of colloid-surface interactions was included for CML and collector surfaces with RMS roughness greater than 4 nm, following the characterization described in Rasmuson et al.[29] The silica collector surface was considered smooth, since its RMS roughness was < 1.0 nm.[29] For the CML, the RMS roughness used in simulations and slip layer effects were estimated as in Rasmuson et al.[29] (SI, Table SI-3).

Discrete Representation of Nanoscale Heterogeneity (DRNH)

Simulations regarding CML attachment under unfavorable conditions were performed by incorporating DRNH on the silica collector surface. Heterodomains of specified size were "placed" at intervals in polar coordinate space (r and θ) from the impinging jet axis to generate uniformly spaced DRNH over the collector surface, as described and demonstrated in Pazmino et al.[12] This discrete representation of heterodomain sizes intends to approximate the

expected continuous size distribution resulting from random clustering of nanoscale physical and chemical features.[26,27,36–38]

The linear superposition approximation (LSA) integration technique was used to calculate colloid-collector surface interactions. For the colloid size analyzed in this study, the influence of the curvature of the colloid and collector surfaces within the ZOI is negligible.[14] Net colloid-collector interaction can therefore be determined by the sum of attractive and repulsive contributions without regard to their specific locations within the ZOI.[12,26]

For simplicity, heterodomain ζ-potentials were assumed to be of equal magnitude and opposite charge to bulk collector surface. This simplification is reasonable given that once the fraction of the ZOI occupied by heterodomain(s) is large enough to yield a net attractive interaction, η is relatively insensitive to the magnitude of the attractive ζ-potential.[12] However, in contrast to η, CML detachment was sensitive to heterodomain ζ-potential, as we describe below.

Results

Experimentally-observed colloid attachment (quantified as collector efficiency, η) in impinging jet experiments showed a characteristic minimum for the n-μ transition CML (Figure 1, symbols). The observed minimum η was exaggerated under unfavorable (Figure 1, red symbols) relative to favorable (Figure 1, blue symbols) conditions. The magnitude of this exaggeration increased with increasing pH (Figure 1, a & b versus c & d) and decreasing IS (Figure 1, a & c versus b & d). The least unfavorable condition (20.0 mM pH 6.7) showed a factor of four exaggerated minimum relative to favorable (Figure 1, a). The most unfavorable condition (6.0 mM pH 8.0) showed a factor of 250 exaggerated minimum relative to favorable (Figure 1, d). These results demonstrate that the exaggerated minimum observed for CML on silica at pH 8.0 and IS of 6.0 mM NaCl[6] also occurs over a broader range of pH and IS conditions, and deepens with increasing unfavorability. Furthermore, η values observed under unfavorable relative to favorable conditions were similar or equivalent for the < 0.2 μm and > 2 μm CML sizes, for all pH and IS conditions examined (Figure 1, symbols), suggesting that the

greater combined diffusion and settling for these colloids counteracted colloid-collector repulsion under unfavorable conditions.

To explore our primary hypothesis that the exaggerated minimum η for n-μ transition colloids is driven by their interaction with nanoscale heterodomains on surfaces, we simulated colloid attachment on the collector surface under unfavorable conditions via incorporation of DRNH. Heterodomain sizes and spatial densities in mechanistic Lagrangian particle trajectory simulations (full force and torque balance) were optimized to simulate η values that matched experiments (Figure 1, lines). Heterodomain radius was set to a fraction (0.48) of the square root of colloid radius (approximating RZOI independent of ionic strength[26]). This fraction was constrained to match experimentally-observed attachment (η) at a particular IS (6.0 mM) and pH (6.7), as well as detachment of 0.25 μm CML in response to IS perturbation.[29,33]

A near-Power law (geometric with non-zero asymptote) distribution of heterodomain spatial density versus heterodomain size emerged from the above calibration and was described by a power law function with a non-zero asymptote (Figure 2), consistent with previous work that examined a relatively narrow CML size distribution (0.25 to 2.0 μm).[12,13] The heterodomains ranged in size from 40 to 320 nm, for 0.1 to 6.8 μm CML, with corresponding spatial densities (SD) ranging from 7.0×10^6 to 4.0×10^2 per mm^2, respectively (Figure 2). Heterodomain SD decreased with increasing pH (Figure 2), also consistent with previous work.[13] The resulting DRNH was found to predict CML attachment for IS conditions other than those used to constrain it (e.g., 20.0 mM), as described below, as well as CML detachment in response to IS and flow perturbations[29,33], and also further described below.

Mechanistic trajectory simulations incorporating DRNH yielded the characteristic minimum η observed for n-μ transition colloids in experiments (Figure 1, lines). Whereas heterodomain sizes (Figure 2) were optimized using data from pH 6.7, IS 6.0 mM conditions, the simulated η values were in good agreement with experimentally-observed η across the range of colloid sizes (0.1 to 6.8 μm) for the higher IS condition (20.0 mM), wherein the IS influence on EDL interactions mechanistically drove the response of simulations (η) to IS. The match was also

good for both IS conditions at the higher pH (8.0) wherein a single reduced value of SD was adopted (Figure 2) consistent with the well-known direct relationship between negative ζ-potential and pH for silicate minerals[13] resulting from protonation/deprotonation of oxide moieties. Under-predicted η values corresponding to the largest colloid sizes (Figure 1, lines versus symbols) are addressed further below.

As observed in experiments, the simulated minimum η was exaggerated under unfavorable conditions (Figure 1, red dashed line) relative to favorable conditions (Figure 1, blue solid line). Exaggeration of simulated minimum η increased with increased pH (Figure 1, a & b versus c & d) and decreased IS (Figure 1, a & c versus b & d) in correspondence with observations.

For < 0.2 μm CML, simulated η values were similar under unfavorable and favorable conditions regardless of pH and IS condition, in correspondence with experimental observations (Figure 1 lines). In contrast, for > 2 μm CML, simulated η values remained a factor of four to 50 reduced under unfavorable relative to favorable conditions for the least unfavorable (20.0 mM pH 6.7) (Figure 1 a) and most unfavorable (6.0 mM pH 8.0) (Figure 1 d) conditions, respectively.

Discussion

Effects of combined diffusion, settling and fluid drag.

Our primary hypothesis, that the exaggerated minimum η observed for n-μ transition colloids under unfavorable conditions is driven by their least-combined diffusion, settling, and fluid drag is examined via characteristics recorded in their simulated trajectories (Figure 3); specifically their simulated mean residence times prior to attachment (Figure 3 d). Simulated residence time prior to attachment included time spent in: 1) the bulk fluid domain ; 2) the near-surface fluid domain corresponding to significant van der Waals (vdW) interaction (also commonly referred to as secondary minimum interactions); and 3) the contact domain wherein the contact mechanics torque balance in the primary minimum determines whether arrest (attachment) occurs.[33] Residence times in all three of these domains were recorded in the numerical simulations. Simulated residence times prior to attachment were greater under

unfavorable (Figure 3 red triangles) relative to favorable (Figure 3 blue circles) conditions, as driven by increased near-surface and contact residence times under unfavorable conditions, as further explored below. Simulated total residence time prior to attachment was greatest for *n*-μ transition CML regardless of whether conditions were favorable (Figure 3 d, blue circles) versus unfavorable (Figure 3 d, red triangles).

Conceptually, mean residence times prior to attachment are inversely proportional to attachment rate constants (k_f).[39] The proportionality of η to k_f dictates that the greater residence time for *n*-μ transition CML corresponds to their minimum η, which is well known to be driven by their least-combined diffusion and settling. That *n*-μ transition CML showed greater residence times also under unfavorable conditions suggests an influence of diffusion and settling on CML residence time prior to attachment under unfavorable conditions. However, upon reaching the near-surface environment (< 200 nm separation distance), the likelihood of encountering heterodomains is no longer driven by settling, but rather by diffusion and fluid drag, as described below.

Enhanced residence times under unfavorable relative to favorable conditions (Figure 3 b, red triangles versus blue circles) reflect increased near-surface residence times wherein translation in secondary minimum-association with the surface occurs until a heterodomain(s) is encountered that occupies a sufficient fraction of the ZOI to arrest the colloid. Lack of secondary minimum-association is characteristic of < 0.25 μm colloid trajectories (Figure 3 a, blue trajectory) wherein their trajectories were dominated by separation distances exceeding 200 nm. Diffusion was evident not only in the normal dimension but also in the radial dimension which enhanced their likelihood of encountering heterodomains (Figure 3 a, blue trajectory).

Because forces scale with colloid size, trajectories for n-μ transition and larger CML were characterized by persistent secondary minimum attraction that held colloids in the near-surface fluid domain (Figure 3 a, red and green trajectories). Notably, near-surface residence times were greatest for n-μ transition CML despite secondary minimum interaction being greater for

larger CML (Figure 3 a). Larger CML experienced shorter near-surface residence times prior to attachment (relative to n-μ transition CML) because their enhanced fluid drag moved them faster toward heterodomains in their path. This is demonstrated by the larger radial distance traveled in the near-surface fluid domain over a shorter time period for larger CML relative to n-μ transition CML (Figure 3 a, green versus red trajectories). The greater near surface residence time for n-μ transition CML under unfavorable conditions (Figure 3 a) therefore reflects their least combined diffusion and fluid drag, as demonstrated by near-surface trajectories (Figure 3 a, red trajectory).

The greater total residence time (bulk fluid and near-surface domains) of n-μ transition CML under unfavorable conditions (Figure 3 b, red triangles) is driven by their least combined diffusion and settling which reduces their likelihood of delivery to the near surface (Figure 3 b, blue circles) and their least combined diffusion and fluid drag which reduces their likelihood of encountering heterodomains on which to arrest. Hence, these physical processes (diffusion, settling and fluid drag) impact transport in the bulk fluid and near-surface domains to produce the observed exaggerated η under unfavorable conditions (Figure 1).

Near-Power law DRNH to represent a continuum distribution

Inherently heterogeneous surfaces can be expected to host a continuum of heterodomain sizes ranging from a given primary size that randomly cluster, to form progressively larger and less frequent heterodomains. The nature of the primary size of heterodomains can reflect, for example chemical substitutions or crystalline defects. Amorphous silica glasses include Na, Ca, K, Mg, Al, and other impurities[40,41] in both surface and bulk domains.[23,42,43] Heterogeneity at scales and spatial distribution relevant to colloidal transport has been generated using cationic polymers[27,36–38] and simulated using random placement of primary heterodomains (11 nm in diameter) on surfaces to recreate nanoscale heterogeneity.[26] Random placement produces a geometric distribution in which the frequency of a given heterodomain decreases according to a power-law function of its size. Simulations using random placement of primary heterodomains yielded colloid attachment onto clusters.[26] Discrete heterodomain sizes comprising the DRNH used in this work (Figure 2) explicitly represents clustering. While DRNH

uses a single heterodomain size to arrest and release a given-sized colloid, this is a discrete representation of the continuum of actual heterodomains (a subset of the larger continuum) that can capture and release colloids of that given size under the examined experimental conditions. As such, the spatial density corresponding to a given discrete heterodomain size accounts for the summed spatial densities of individuals in the actual subset continuum (Figure 2, dashed lines).

We find that superimposing discrete heterodomain sizes and spatial densities onto a single surface while conforming their relationship to a power-law distribution does not capture experimental results for both attachment and detachment. For example, DRNH using power law-distributed heterodomains of three different sizes (220, 40, and 25 nm) increasing frequency ratios (1:8:64) superimposed onto a single surface (SI, Figure SI-3), produced excellent fit to experimentally-observed CML attachment (η) across the size range examined in this study (0.1 to 6.8 μm) (Figure 4 a, lines), and captured the observed exaggerated minimum under unfavorable conditions. However, this DRNH did not capture CML detachment in response to IS perturbation (Figure 4 b, lines) for the 0.25 μm CML. Non-target capture of 0.25 μm CML by 25 nm heterodomains (for which 0.1 μm CML were targeted for arrest) drove their over-predicted detachment (under-predicted % remaining) in response to IS reduction. DRNH superimposed onto a single surface failed to comprehensively predict attachment and detachment experiments because it identifies a given heterodomain size to represent what is actually an underlying continuum (Figure 2, dashed lines), and because natural distributions may not strictly follow Pareto or other power-law functions.

Sensitivity to heterodomain size was also demonstrated by dramatic η decreases in response to reducing 220 to 110 nm, and 25 to 15 nm, for the 0.1 μm and > 2 μm, respectively (Figure 4, dotted red line). The near-Power law relationship between heterodomain spatial density and heterodomain size yields the experimentally-observed exaggerated minimum η despite this relationship having no minimum corresponding to the n-μ transition colloid size (Figure 2). This further highlights that the experimentally-observed exaggerated minimum η emerges from the

transport simulations, due to the impacts of diffusion, settling, and fluid drag, as described above.

Sensitivity to order-of-magnitude decreased heterodomain spatial density in response to pH increase from 6.7 to 8.0 (Figure 2, blue versus red lines) is demonstrated by decreased simulated η (Figure 1, a & b versus c & d red lines). Decreased spatial density with increased pH was also demonstrated for other mineral surfaces (muscovite and albite) using the methods described in this paper for a narrower colloid size range.[12,13]

Generalizing the exaggerated minimum for n-μ transition colloids

Our leveraged simulations and experiments expand the range of CML sizes addressed under unfavorable attachment conditions using DRNH across nano- to micro-scales (0.1 to 6.8 μm CML) and under a range of pH and IS conditions. Previous work examining the role of heterogeneity on colloids versus collectors focused on 1 μm sized colloids[27], raising two questions: a) whether the faster kinetics of attachment for heterogeneity on the collector applies to colloid sizes smaller and larger than 1 μm; and b) whether the exaggerated minimum that we observed and explained for n-μ transition CML applies to colloids with contrasting hydrophobicity and rheology, such as the silica colloids examined by Shave et al.[27]

To allow comparison between colloids of differing densities (silica versus polystyrene), with contrasting contributions of settling to η, we use the ratio of η under unfavorable to favorable conditions (Figure 1), referred to as attachment (or collision) efficiency ($\alpha = \eta_{unf}/\eta_{fav}$) (Figure 5). The exaggerated minimum η (Figure 1) corresponds to a minimum α for the *n*-μ transition CML (Figure 5, open circles and triangles). This minimum deepens as pH increases (Figure 5, dashed versus solid lines), and as IS decreases (Figure 5, circles versus triangles) (Figure 5); i.e., minimum α decreases with increasing unfavorability. In contrast to n-μ transition CML, the < 0.2 and > 2 μm CML α values approached unity (Figure 5) regardless of unfavorability.

Notably, polar (non-hydrophobic) unmodified silica (UMS) colloids (3.0 μm) yielded α values approaching unity (Figure 5, patterned triangle) under unfavorable attachment conditions (pH =

6.7, IS = 6.0 mM), demonstrating that properties specific to CML (e.g., hydrophobicity) did not drive the observed *ca.* unity α values for > 2 μm CML. Near-unity α was also observed for 3.0 μm carboxylate-modified silica (CMS) colloids (Figure 5, solid triangle), which were tested because of potential hydrophobicity introduced via silane linkage of carboxyl functionality to silica. In contrast to 3.0 μm CMS, 1.0 μm CMS yielded an α value a factor of 40 below unity (0.025) (Figure 5, patterned triangles), demonstrating that CMS showed reduced α for n-μ transition size range, similar to CML, and demonstrating that the exaggerated minimum α observed for n-μ transition CML occurs for colloids of contrasting hydrophobicity and rheology, and that the impact of least combined diffusion, settling, and fluid drag on colloid attachment is a general phenomenon. We note that the expense and lower fluorescence quantum yield (optical clarity) for UMS and CMS limited our experiments to silica colloids exceeding 0.5 μm in size.

Simulated η values for > 2 μm CML differed under favorable versus unfavorable conditions, in contrast to experiments (Figure 1), demonstrating that the simulations did not account for a property of these larger colloids. Experiments comparing UMS, CMS, and CML demonstrated that exaggerated minima are general among these colloids, and that whatever property is missing in our simulations to account for α values approaching unity for > 2 μm colloids, is general to UMS, CMS, and CML. Future work will examine the potential role of heterogeneity on colloidal surfaces as the source of the discrepancy between simulations and experimental observations for > 2 μm colloids.

To further examine the generality of the observed exaggerated minimum α for n-μ transition colloids, we compiled reported values of colloid attachment (as η or k_f) from the published literature for transport studies of non-biological and biological colloids on silica or quartz sand packed columns, with media having well sorted and well characterized size distribution, pH in the range 5 < pH < 10, and detection methods that would account for all colloids (live and dead in the case of biological colloids). Attachment efficiency (α) was determined from the ratio of reported attachment under unfavorable relative to favorable conditions, with calculation of favorable values from a correlation equation[44] for η when favorable values were not reported

(Table SI-4). Correlation equations and underlying theory are approximations of reality, and as such have inherent error. Hence, for systems approaching favorable, calculated attachment efficiencies (α) may exceed unity."

Compiled data from environmental transport literature also indicates that α is minimal for *n*-μ transition colloids, indicating that it is a general phenomenon spanning engineered nanomaterials (ENP), viruses, bacteria and protozoa (microbes), carboxylate modified silica (CMS), and CML (Figure 6). Whereas there is a great deal of overlap among data from different conditions, a general trend emerges wherein the highest α values circumscribe a trend of relatively lower α values for n-μ transition colloids, specifically ~ 0.5 μm in this collection of porous media data. Values of α vary widely for any given colloid size, at least in part due to surface property and solution condition differences among experiments (Figure 6).

Significance

In Figure 6, viruses (0.02 to 0.065 μm) display particularly low attachment, likely contributing to their generally greater prevalence in groundwater,[45,46] as well as the misperception that smaller colloids transport over farther distances. Our experimental and simulation results highlight that the relatively low α associated with viruses arises not from their small size, but rather their surface properties that prevent attachment. The low attachment of viruses highlights a strategy for strict mobility; whereas, our combined experiments, simulations and literature compilation suggest that for the purposes of targeted delivery, an over-looked strategy, particularly for near neutrally-buoyant colloids, is aggregation to the relatively mobile micro-sized interval to minimize attachment in non-target media, followed by disaggregation, or further aggregation, to maximize retention on target media. Our experimental results and simulations demonstrate that while a modest form of this outcome is already expected under favorable conditions, it can be greatly enhanced under unfavorable interactions that dominate in environmental contexts, offering the potential to tune colloid sizes to harness nanoscale interactions to optimize transport and retention for targeted colloid delivery. Incorporation of DRNH to account for nanoscale surface heterogeneity serves as a guide to future investigations

utilizing spectrometric, potentiometric and other techniques for direct surface characterization. Specifically, it identifies the expected scales and spatial frequencies of the relevant nanoscale heterogeneities. Notably, the DRNH approach utilized here was previously demonstrated to describe colloid attachment to mineral surfaces other than soda-lime glass (albite and muscovite).[13] Understanding the influences of nanoscale heterogeneity holds promise for tuning engineered heterogeneous surfaces for desired transport and attachment outcomes, which can also be moderated by solution conditions (e.g., IS, pH, fluid velocity).

Another significance of our findings is that while α has traditionally been generalized to reflect "chemical" influences, η has traditionally been generalized to reflect "physical" influences. Our findings demonstrate that these are over-generalizations; physical mass transport in the near-surface fluid domain under unfavorable conditions governs attachment; η concerns colloid transport in bulk fluid, whereas α concerns colloid transport in near surface fluid.

Our model incorporating DRNH approximates the physics/chemistry of a complex system, but it is a major improvement on the current state of colloid transport science and practice, which lacks easily implemented prediction of colloid retention under unfavorable conditions. It is well known that the mechanistic driver of colloid attachment under unfavorable conditions is nanoscale heterogeneity. We have successfully parameterized a mechanistic relationship between colloid retention and nanoscale heterogeneity represented via ζ-potential. Of course there's fitting involved, as there always is when characteristics are not directly measurable. However, our fitting occurs at an unprecedented fundamental level that allows observed behaviors to emerge from the underlying mechanistic processes. Not only do the attachment and detachment behaviors emerge, but also the minimum α that constitutes a novel transport behavior, the observed exaggerated minimum η under unfavorable conditions. Whereas application of this approach in natural porous media is a topic of future work, we note that residence time distributions simulated under favorable versus unfavorable conditions in a Happel sphere-in-cell collector representing porous media[7] predicted experimentally-observed non-log-linear distributions of retained colloids with distance from source under unfavorable conditions in media composed of spheroidal grains.[39] The efficiencies extracted from the

residence time distributions yielded continuum-scale coefficients (via upscaling) that effectively produced fast- and slow-attaching subfractions from which emerged hyperexponential and nonmonotonic profiles of retained colloids.

To facilitate exploration of exaggerated minimum η for n-μ transition colloids, and related phenomena, we provide executable codes at: http://www.wpjohnsongroup.utah.edu > Research > Downloads.

Conflicts of interest

Authors declare no conflict of interest.

Acknowledgements

This article is based upon work supported by the National Science Foundation Program: Designing Materials to Revolutionize and Engineer our Future (DMREF) (1629078). Any opinions, findings, and conclusions or recommendations expressed in this material are those of the authors and do not necessarily reflect the views of the National Science Foundation. We are also grateful for the technical and facility support provided at the Center for High Performance Computing (CHPC) at the University of Utah.

References

1 M. Elimelech and C. R. O'Melia, Kinetics of Deposition of Colloidal Particles in Porous Media, *Environ. Sci. Technol.*, 1990, **24**, 1528–1536.

2 C. H. Bolster, A. L. Mills, G. M. Hornberger and J. S. Herman, Spatial distribution of deposited bacteria following miscible displacement experiments in intact cores, *Water Resour. Res.*, 1999, **35**, 1797–1807.

3 J. A. Redman, M. K. Estes and S. B. Grant, Resolving macroscale and microscale heterogeneity in virus filtration, *Colloids Surfaces A Physicochem. Eng. Asp.*, 2001, **191**, 57–70.

4 N. Tufenkji and M. Elimelech, Deviation from the Classical Colloid Filtration Theory in the Presence of Repulsive DLVO Interactions, *Langmuir*, 2004, **20**, 10818–10828.

5 X. Li, T. D. Scheibe and W. P. Johnson, Apparent Decreases in Colloid Deposition Rate Coefficients with Distance of Transport under Unfavorable Deposition Conditions: A General Phenomenon, *Environ. Sci. Technol.*, 2004, **38**, 5616–5625.

6 A. Rasmuson, E. Pazmino, S. Assemi and W. P. Johnson, Contribution of Nano- to Microscale Roughness to Heterogeneity: Closing the Gap between Unfavorable and Favorable Colloid Attachment Conditions, *Environ. Sci. Technol.*, 2017, **51**, 2151–2160.

7 R. Rajagopalan and C. Tien, Trajectory analysis of deep-bed filtration with the sphere-in-cell porous media model, *AIChE J.*, 1976, **22**, 523–533.

8 M. Elimelech, Particle deposition on ideal collectors from dilute flowing suspensions: Mathematical formulation, numerical solution, and simulations, *Sep. Technol.*, 1994, **4**, 186–212.

9 K. Yao, M. T. Habibian and C. R. O'Melia, Water and Waste Water Filtration: Concepts and Applications, *Environ. Sci. Technol.*, 1971, **5**, 1105–1112.

10 M. Tong and W. P. Johnson, Excess colloid retention in porous media as a function of colloid size, fluid velocity, and grain angularity, *Environ. Sci. Technol.*, 2006, **40**, 7725–7731.

11 E. Pazmino, H. Ma and W. P. Johnson, Applicability of Colloid Filtration Theory in Size-Distributed, Reduced Porosity, Granular Media in the Absence of Energy Barriers, *Environ. Sci. Technol.*, 2011, **45**, 10401–10407.

12 E. Pazmino, J. Trauscht, B. Dame and W. P. Johnson, Power Law Size-Distributed Heterogeneity Explains Colloid Retention on Soda Lime Glass in the Presence of Energy Barriers, *Langmuir*, 2014, **30**, 5412–5421.

13 J. Trauscht, E. Pazmino and W. P. Johnson, Prediction of Nanoparticle and Colloid Attachment on Unfavorable Mineral Surfaces Using Representative Discrete Heterogeneity, *Langmuir*, 2015, **31**, 9366–9378.

14 M. Bendersky and J. M. Davis, DLVO interaction of colloidal particles with topographically and chemically heterogeneous surfaces, *J. Colloid Interface Sci.*, 2011, **353**, 87–97.

15 S. Bhattacharjee, C.-H. Ko and M. Elimelech, DLVO Interaction between Rough Surfaces, *Langmuir*, 1998, **14**, 3365–3375.

16 J. Drelich and Y. U. Wang, Charge heterogeneity of surfaces: Mapping and effects on surface forces, *Adv. Colloid Interface Sci.*, 2011, **165**, 91–101.

17 R. Duffadar and J. M. Davis, Interaction of micrometer-scale particles with nanotextured surfaces in shear flow, *J. Colloid Interface Sci.*, 2007, **308**, 20–29.

18 R. Vaidyanathan and C. Tien, Hydrosol deposition in granular media under unfavorable surface conditions, *Chem. Eng. Sci.*, 1991, **46**, 967–983.

19 P. R. Johnson and M. Elimelech, Dynamics of Colloid Deposition in Porous Media: Blocking Based on Random Sequential Adsorption, *Langmuir*, 1995, **11**, 801–812.

20 M. Elimelech, M. Nagai, C. H. Ko and J. N. Ryan, Relative insignificance of mineral grain zeta potential to colloid transport in geochemically heterogeneous porous media, *Environ. Sci. Technol.*, 2000, **34**, 2143–2148.

21 K. Shellenberger and B. E. Logan, Effect of molecular scale roughness of glass beads on colloidal and bacterial deposition, *Environ. Sci. Technol.*, 2002, **36**, 184–189.

22 P. Taboada-Serrano, V. Vithayaveroj, S. Yiacoumi and C. Tsouris, Surface charge heterogeneities measured by atomic force microscopy, *Environ. Sci. Technol.*, 2005, **39**, 6352–6360.

23 E. Metwalli, D. Haines, O. Becker, S. Conzone and C. G. Pantano, Surface

characterizations of mono-, di-, and tri-aminosilane treated glass substrates, *J. Colloid Interface Sci.*, 2006, **298**, 825–831.

24 R. Charmas, P. Zarzycki, F. Villiéras, F. Thomas, B. Prélot and W. Piasecki, Influence of electrolyte ion adsorption on the derivative of potentiometric titration curve of oxide suspension - Theoretical analysis, *Colloids Surfaces A Physicochem. Eng. Asp.*, 2004, **244**, 9–17.

25 B. Prélot, F. Villiéras, M. Pelletier, G. Gérard, F. Gaboriaud, J.-J. Ehrhardt, J. Perrone, M. Fedoroff, J. Jeanjean, G. Lefèvre, L. Mazerolles, J.-L. Pastol, J.-C. Rouchaud and C. Lindecker, Morphology and surface heterogeneities in synthetic goethites, *J. Colloid Interface Sci.*, 2003, **261**, 244–254.

26 R. Duffadar, S. Kalasin, J. M. Davis and M. M. Santore, The impact of nanoscale chemical features on micron-scale adhesion: Crossover from heterogeneity-dominated to mean-field behavior, *J. Colloid Interface Sci.*, 2009, **337**, 396–407.

27 M. K. Shave, S. Kalasin, E. Ying and M. M. Santore, Nanoscale Functionalized Particles with Rotation-Controlled Capture in Shear Flow, *ACS Appl. Mater. Interfaces*, 2018, **10**, 29058–29068.

28 H. Ohshima, Electrophoresis of soft particles: Analytic approximations, *Electrophoresis*, 2006, **27**, 526–533.

29 A. Rasmuson, K. VanNess, C. Ron and W. P. Johnson, Hydrodynamic versus Surface Interaction Impacts of Roughness in Closing the Gap between Favorable and Unfavorable Colloid Transport Conditions, *Environ. Sci. Technol.*, 2019, **53**, 2450–2459.

30 W. Kern and D. A. Puotinen, Interview with W. Kern, *RCA Rev.*, 1970, **31**, 187–206.

31 B. J. Kirby and E. F. Hasselbrink, Zeta potential of microfluidic substrates: 1. Theory, experimental techniques, and effects on separations, *Electrophoresis*, 2004, **25**, 187–202.

32 H. Ma, E. Pazmino and W. P. Johnson, Surface heterogeneity on hemispheres-in-cell model yields all experimentally-observed non-straining colloid retention mechanisms in porous media in the presence of energy barriers, *Langmuir*, 2011, **27**, 14982–14994.

33 K. VanNess, A. Rasmuson, C. A. Ron and W. P. Johnson, Unified Theory for Colloid Transport: Predicting Attachment and Mobilization under Favorable and Unfavorable Conditions, *Langmuir*. In Review.

34 E. M. V. Hoek and G. K. Agarwal, Extended DLVO interactions between spherical particles and rough surfaces, *J. Colloid Interface Sci.*, 2006, **298**, 50–58.

35 S. Torkzaban and S. A. Bradford, Critical role of surface roughness on colloid retention and release in porous media, *Water Res.*, 2016, **88**, 274–284.

36 N. Kozlova and M. M. Santore, Manipulation of Micrometer-Scale Adhesion by Tuning Nanometer-Scale Surface Features, *Langmuir*, 2006, **22**, 1135–1142.

37 S. Kalasin and M. M. Santore, Hydrodynamic Crossover in Dynamic Microparticle Adhesion on Surfaces of Controlled Nanoscale Heterogeneity, *Langmuir*, 2008, **24**, 4435–4438.

38 M. M. Santore and N. Kozlova, Micrometer Scale Adhesion on Nanometer-Scale Patchy Surfaces: Adhesion Rates, Adhesion Thresholds, and Curvature-Based Selectivity, *Langmuir*, 2007, **23**, 4782–4791.

39 W. P. Johnson, A. Rasmuson, E. Pazmiño and M. Hilpert, Why Variant Colloid Transport Behaviors Emerge among Identical Individuals in Porous Media When Colloid–Surface Repulsion Exists, *Environ. Sci. Technol.*, 2018, **52**, 7230–7239.

40 W. H. Zachariasen, The atomic arrangement in glass, *J. Am. Chem. Soc.*, 1932, **54**, 3841–3851.

41 U. K. Krieger and W. A. Lanford, Field assisted transport of Na+ ions, Ca2+ ions and

electrons in commercial soda-lime glass I: Experimental, *J. Non. Cryst. Solids*, 1988, **102**, 50–61.

42 L. L. Hench and D. E. Clark, Physical chemistry of glass surfaces, *J. Non. Cryst. Solids*, 1978, **28**, 83–105.

43 L. C. Bradley, Z. R. Dilworth, A. L. Barnette, E. Hsiao, A. J. Barthel, C. G. Pantano and S. H. Kim, Hydronium Ions in Soda-lime Silicate Glass Surfaces, *J. Am. Ceram. Soc.*, 2013, **96**, 458–463.

44 N. Tufenkji and M. Elimelech, Correlation Equation for Predicting Single-Collector Efficiency in Physicochemical Filtration in Saturated Porous Media, *Environ. Sci. Technol.*, 2004, **38**, 529–536.

45 V. Gupta, W. P. Johnson, P. Shafieian, H. Ryu, A. Alum, M. Abbaszadegan, S. A. Hubbs and T. Rauch-Williams, Riverbank filtration: Comparison of pilot scale transport with theory, *Environ. Sci. Technol.*, 2009, **43**, 669–676.

46 R. C. Bales, S. Li, K. M. Maguire, M. T. Yahya and C. P. Gerba, MS-2 and poliovirus transport in porous media: Hydrophobic effects and chemical perturbations, *Water Resour. Res.*, 1993, **29**, 957–963.

47 E. Pazmino, J. Trauscht and W. P. Johnson, Release of Colloids from Primary Minimum Contact under Unfavorable Conditions by Perturbations in Ionic Strength and Flow Rate, *Environ. Sci. Technol.*, 2014, **48**, 9227–9235.

48 C. Wang, A. D. Bobba, R. Attinti, C. Shen, V. Lazouskaya, L. P. Wang and Y. Jin, Retention and transport of silica nanoparticles in saturated porous media: Effect of concentration and particle size, *Environ. Sci. Technol.*, 2012, **46**, 7151–7158.

49 X. Jiang, M. Tong, R. Lu and H. Kim, Transport and deposition of ZnO nanoparticles in saturated porous media, *Colloids Surfaces A Physicochem. Eng. Asp.*, 2012, **401**, 29–37.

50 L. Liu, Y. Wang, R. Narain and Y. Liu, Functionalized polystyrene microspheres as Cryptosporidium surrogates, *Colloids Surfaces B Biointerfaces*, 2019, **175**, 680–687.

51 N. Tufenkji, G. F. Miller, J. N. Ryan, R. W. Harvey and M. Elimelech, Transport of Cryptosporidium oocysts in porous media: Role of straining and physicochemical filtration, *Environ. Sci. Technol.*, 2004, **38**, 5932–5938.

52 J. A. Redman, S. L. Walker and M. Elimelech, Bacterial Adhesion and Transport in Porous Media: Role of the Secondary Energy Minimum, *Environ. Sci. Technol.*, 2004, **38**, 1777–1785.

53 H. F. Lecoanet, J. Y. Bottero and M. R. Wiesner, Laboratory assessment of the mobility of nanomaterials in porous media, *Environ. Sci. Technol.*, 2004, **38**, 5164–5169.

54 M. Tong, X. Li, C. N. Brow and W. P. Johnson, Detachment-influenced transport of an adhesion-deficient bacterial strain within water-reactive porous media, *Environ. Sci. Technol.*, 2005, **39**, 2500–2508.

55 H. N. Kim and S. L. Walker, Escherichia coli transport in porous media: Influence of cell strain, solution chemistry, and temperature, *Colloids Surfaces B Biointerfaces*, 2009, **71**, 160–167.

56 G. Chen, X. Liu and C. Su, Transport and retention of TiO2 rutile nanoparticles in saturated porous media under low-ionic-strength conditions: Measurements and mechanisms, *Langmuir*, 2011, **27**, 5393–5402.

57 P. Jiemvarangkul, W. X. Zhang and H. L. Lien, Enhanced transport of polyelectrolyte stabilized nanoscale zero-valent iron (nZVI) in porous media, *Chem. Eng. J.*, 2011, **170**, 482–491.

58 Z. Li, E. Sahle-Demessie, A. A. Hassan and G. A. Sorial, Transport and deposition of CeO2 nanoparticles in water-saturated porous media, *Water Res.*, 2011, **45**, 4409–4418.

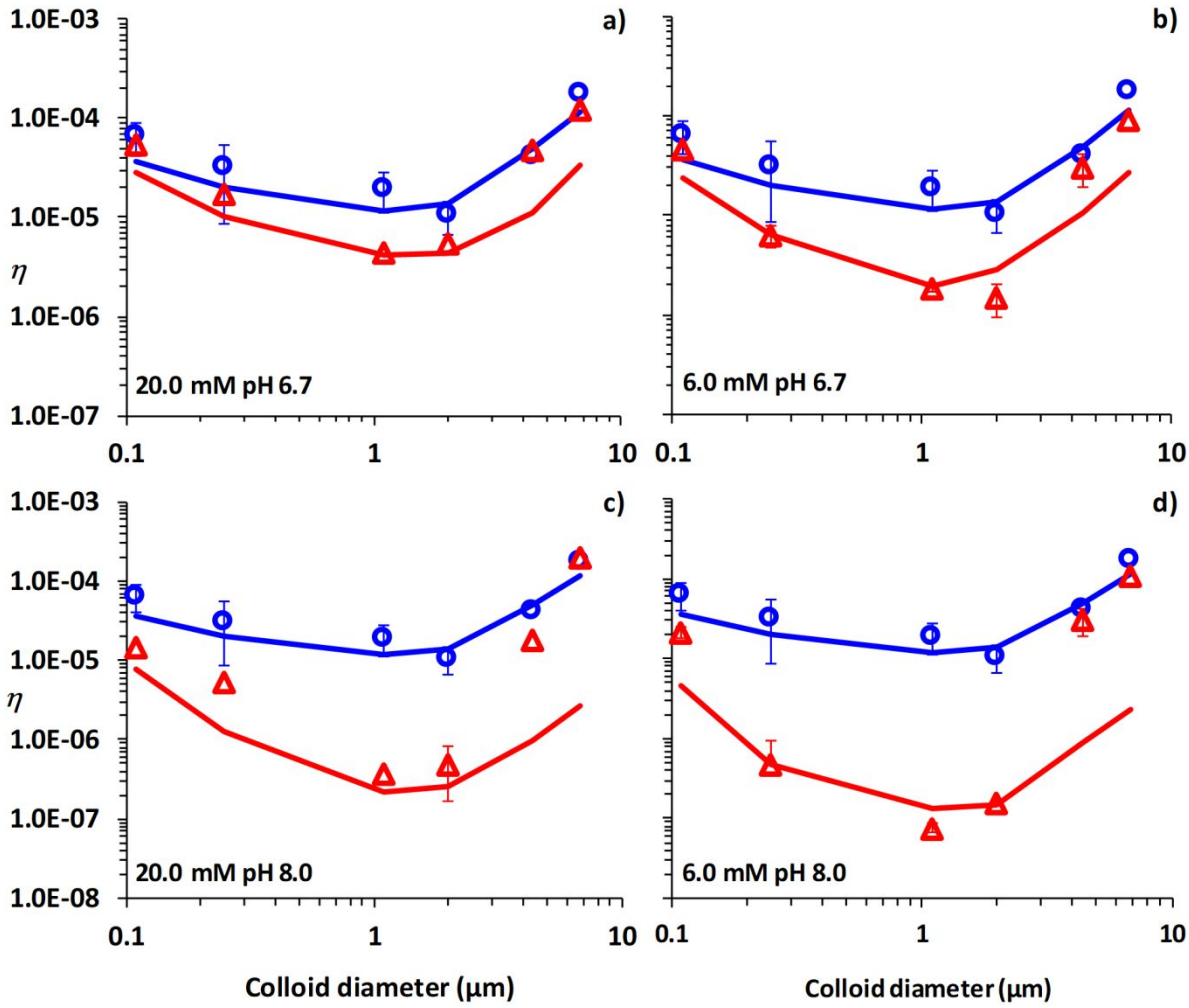

Figure 1. CML collector efficiencies (η) for indicated IS and pH at v_{jet} = 1.7E-3 ms^{-1}. Observed values are denoted by symbols, with blue circles and red triangles corresponding to favorable and unfavorable conditions, respectively. Error bars denote maximum and minimum values for replicate experiments. Solid blue line represents simulations under favorable conditions and solid red line represents simulations under unfavorable conditions.

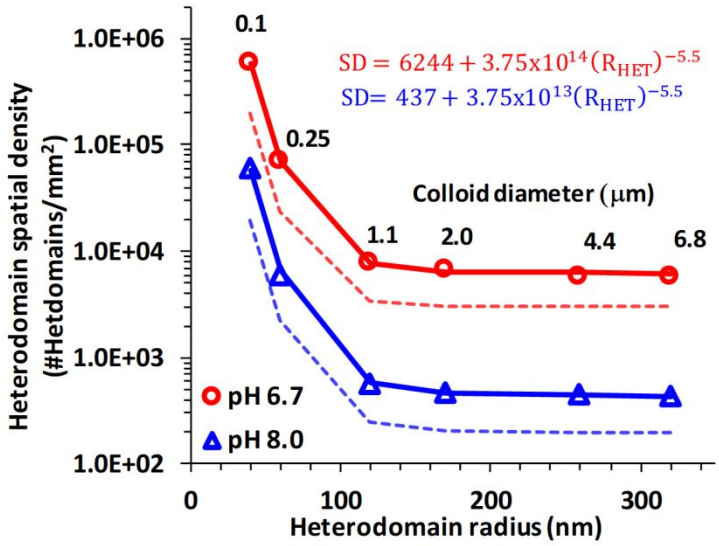

Figure 2. Heterodomain spatial density (# heterodomains per mm^2) utilized in simulations corresponding to pH 6.7 (red circles) and pH 8.0 (blue triangles). Solid lines correspond to asymptotic power law functions (equations shown) fit to discrete values utilized in simulations. Dashed lines schematically represent the underlying continuous distribution represented by discrete values.

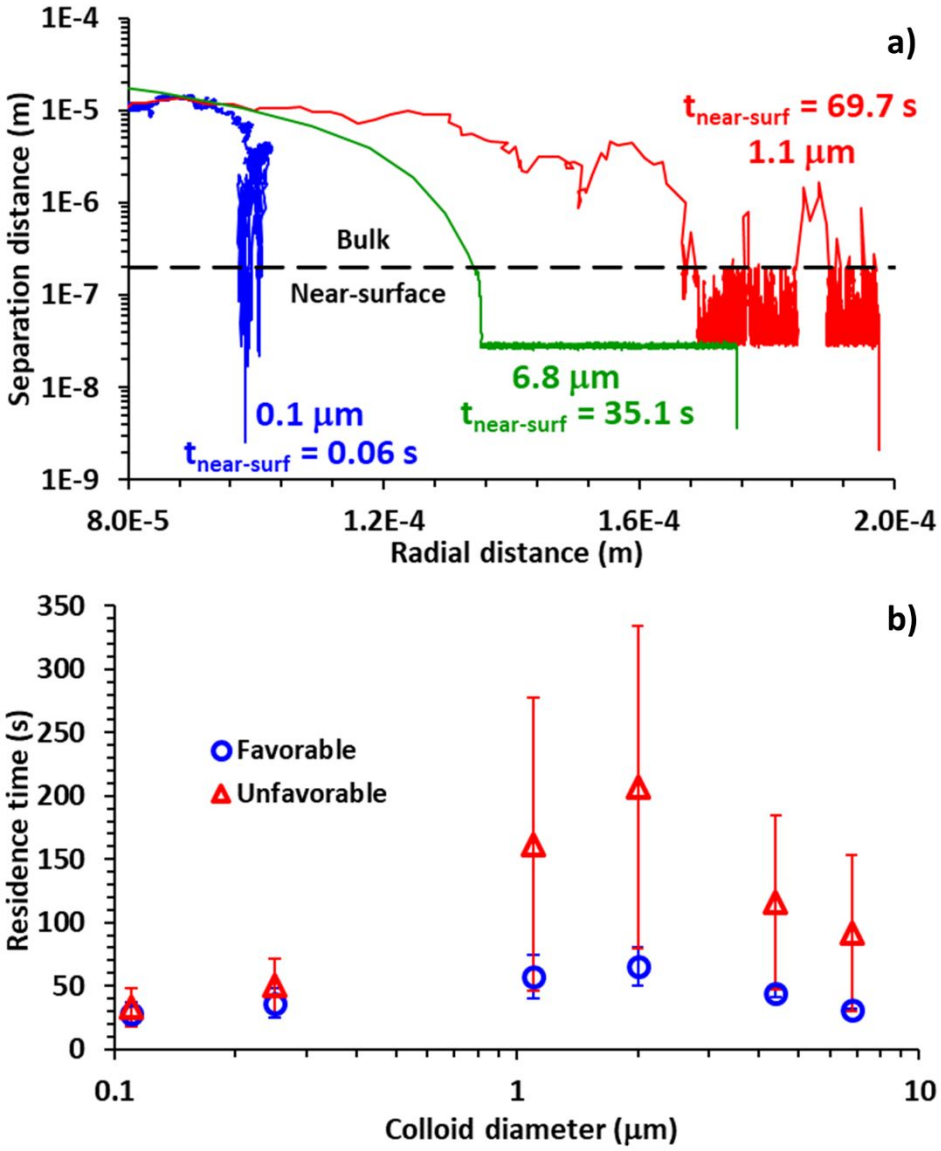

Figure 3. a) Normal view of simulated trajectories for 0.25 µm (blue line), 1.1 µm (red line), and 6.8 µm CML (green line), over an unfavorable collector surface with DRNH as described in Figure 2. Black dashed line divides bulk fluid domain and near-surface fluid domain. b) Simulated mean total residence times of attached colloids under favorable (blue circles) and unfavorable (red triangles) conditions for attachment. Error bars denote maximum and minimum values among the populations of attached colloids. Selected trajectories in panel a) are representative of the mean residence times shown in panel b).

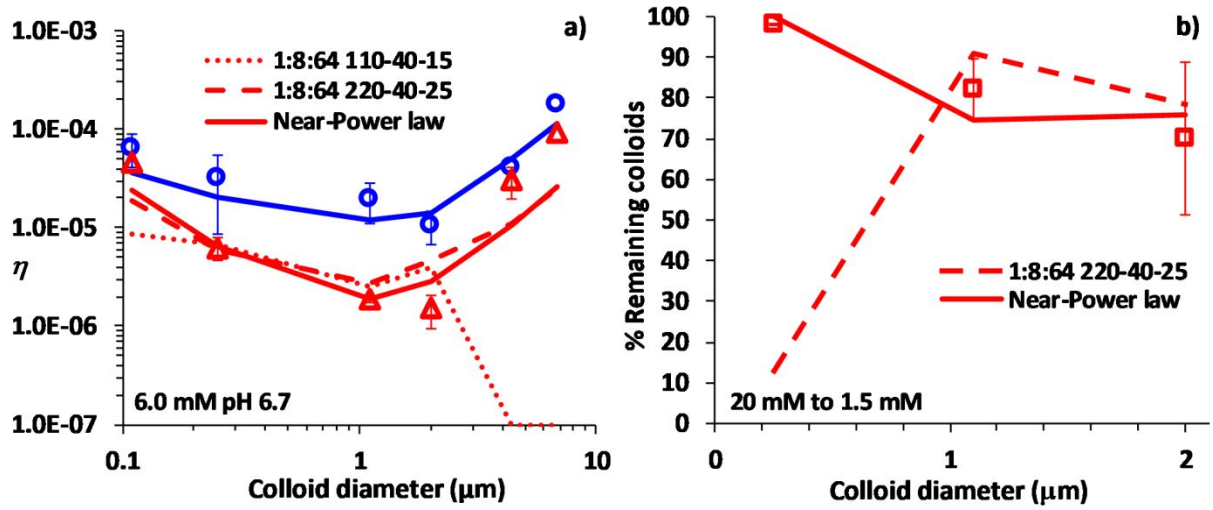

Figure 4. a) Experimental collector efficiencies (η) for 6.0 mM and pH 6.7 at v_{jet} = 1.7E-3 ms^{-1}. Blue circles correspond to favorable conditions and red triangles correspond to unfavorable conditions. Error bars denote maximum and minimum values for replicate experiments. Solid blue line represents simulations under favorable conditions, solid red line represents simulations under unfavorable conditions considering near-Power law DRNH developed in this work, and dashed red lines represent simulations under unfavorable conditions considering Pareto DRNH. b) Experimental percentages of remaining colloids after an IS perturbation (20.0 mM to 1.5 mM) under unfavorable conditions (red squares).[47] Error bars denote maximum and minimum values for replicate experiments. Solid red line represents simulations under unfavorable conditions considering near-Power law DRNH developed in this work, and dashed red lines represent simulations under unfavorable conditions considering 1:8:64 Pareto-distributed 220, 40, and 25 nm heterodomains.

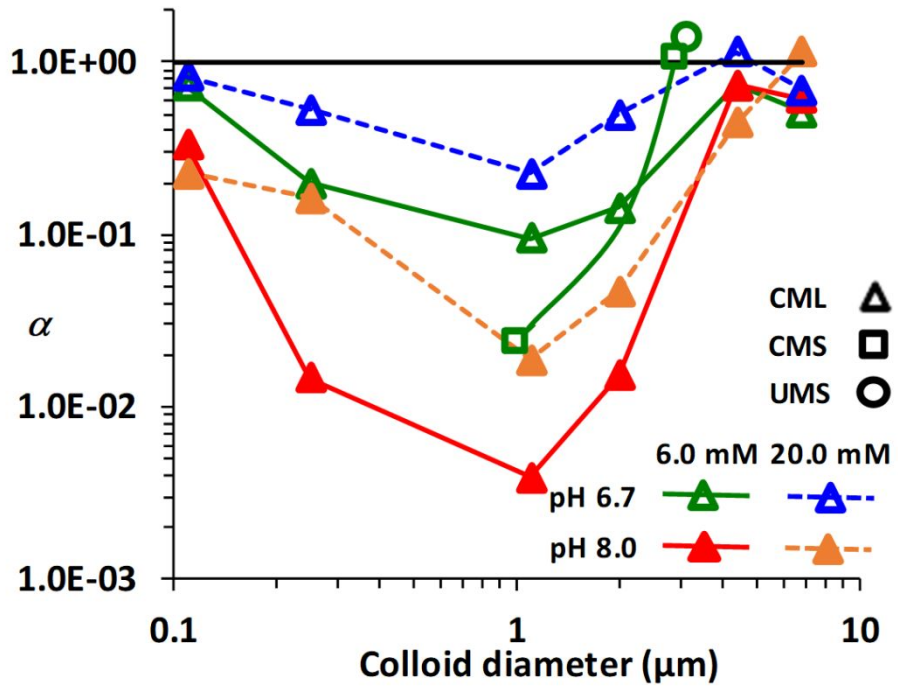

Figure 5. Experimental attachment efficiencies (α) for CML (triangles) versus CMS (squares) and UMS (circles) for pH 6.7 (open symbols), pH 8.0 (solid symbols), 6.0 mM (solid lines) and 20.0 mM (dashed lines) at v_{jet} = 1.7E-3 ms^{-1}. For purposes of differentiation, 3.0 μm CMS and 3.0 μm UMS were represented as 2.9 and 3.1 μm colloids, respectively.

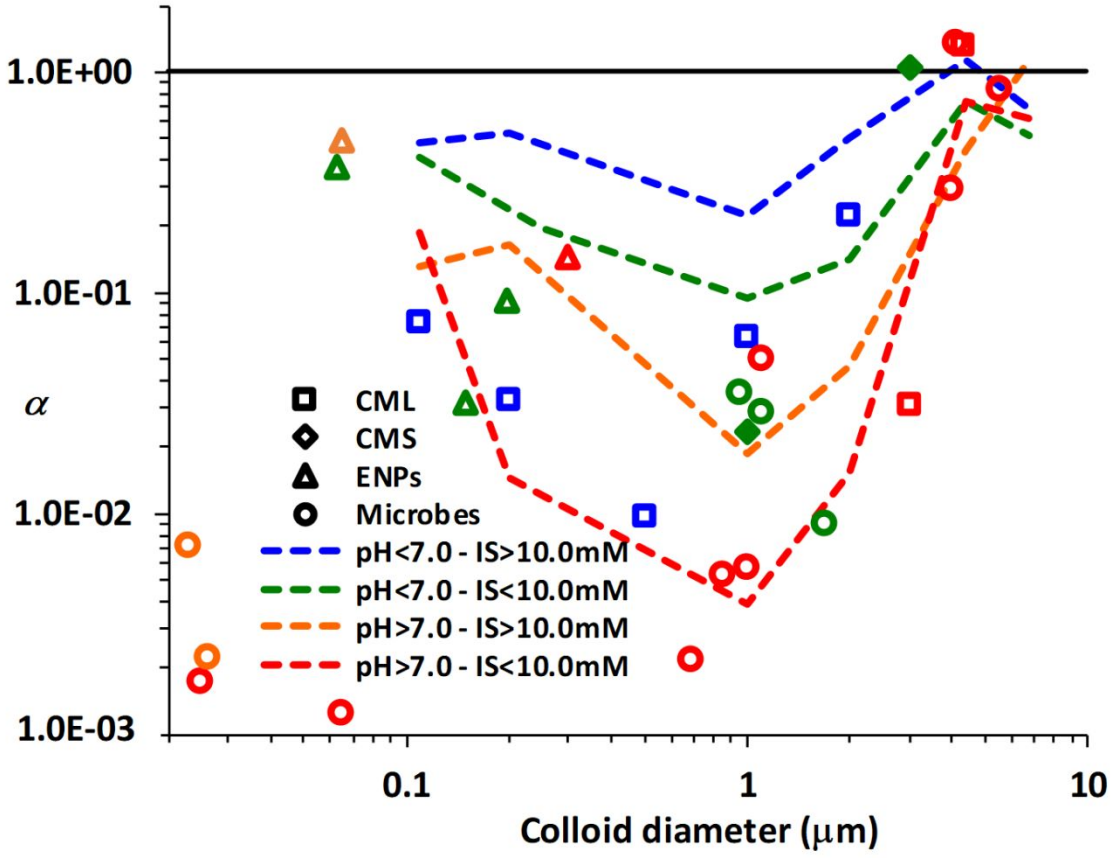

Figure 6. Attachment efficiencies (α) for CML on glass data provided in Figure 1 (shown as lines), augmented with data (shown as symbols) from literature concerning colloid transport in porous media.[10,45,48–58]

Abstract Art